55

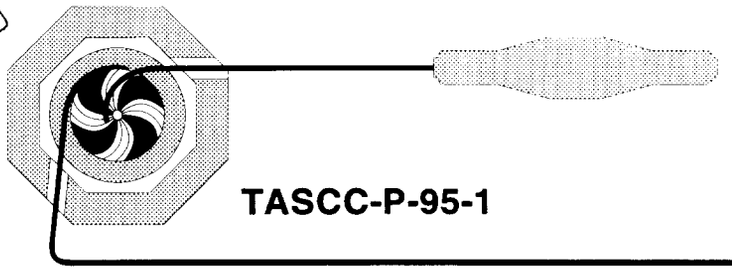

PREPRINT

TASCC-P-95-1

tascc

Dielectronic recombination and energy-loss for He-like ^{79}Br ions channeled in a thin single crystal of Si

J.U. Andersen[a], J. Chevallier[a], G.C. Ball[b], W.G. Davies[b], J.S. Forster[b], J.S. Geiger[b], J.A. Davies[c], H. Geissel[d] and E.P. Kanter[e]

[a]University of Aarhus, DK 8000 Aarhus C, Denmark
[b]AECL Research, Chalk River Laboratories, Chalk River, Ontario, Canada K0J 1J0
[c]McMaster University, Hamilton, Ontario, Canada L8S 4M1
[d]Postfach 11 05 52, D-6100 Darmstadt, Germany
[e]Argonne National Laboratory, Argonne, IL 60439, U.S.A.

Submitted to Phys. Rev. A

Physical and Environmental Sciences
Chalk River Laboratories
Chalk River, ON K0J 1J0 Canada

1995 February

ABSTRACT

Dielectronic recombination (DR) of He-like ^{79}Br ions channeled along the <110> axis of a thin Si crystal has been studied by measurement of charge-state distribution and x-ray production. The results of the charge-state measurements confirm that the probability of resonance capture is proportional to the valence electron density seen by the ion. The energy-loss distributions of channeled ions are also in good agreement with theoretical estimates.

PACS numbers: 34.80.Kw, 34.80.Dp, 61.80.Mk

1. INTRODUCTION

Dielectronic recombination (DR) is a process in which an ion in an electron gas captures an electron with simultaneous excitation of a bound electron i.e., an inverse Auger process. This doubly excited state can decay by Auger emission or be stabilized by emitting a photon. The process is resonant and has a peak cross section when the velocity of the ion matches the velocity of a KLL Auger electron. When the captured electron is initially bound in a target atom, the DR process is often denoted as resonant transfer and excitation (RTE).

The first measurements of RTE were made by Tanis et al.[1] for collisions of S^{13+} ions in an Ar gas. More recently, Datz et al.[2] showed that RTE can be studied using channeling techniques, since heavy ions channeled in thin crystals interact mainly with loosely bound electrons and normal capture in close collisions with atoms is suppressed. Datz et al.[2] measured RTE cross sections for S^{15+}, Ca^{19+}, Ti^{20+} and Ti^{21+} ions channeled in Si crystals by observing x-rays emitted by the doubly-excited ions.

In a similar experiment, Belkacem et al.[3] measured RTE for Ti^{19+} and Ti^{20+} ions channeled along a <110> axis in an Au crystal. The best-channeled ions were selected as those ions with the lowest energy loss. They observed the fraction of ions that captured one electron, as a function of energy, and reported a resonance width five times narrower than any previously observed for RTE. Dittner et al.[4] repeated this measurement for Ti^{20+} ions channeled along a <100> axis in a thin Au crystal; they were

unable to detect any resonance. We have recently measured DR for He-like ^{79}Br ions channeled along a <110> axis in a thin Au crystal[5] and observed a resonance strength and width compatible with the predicted values for an electron gas with a density corresponding to the average electron density in a <110> channel in Au.

Finally, Andriamonje et al.[6] observed the KLL resonance for He-like Xe ions channeled along a <110> axis in Si. They observed the resonance both by detecting photons from the decay of the doubly-excited state and by measuring the energy dependence of charge-state fractions of ions exiting the crystal with lov energy loss. A detailed analysis of the energy loss in these experiments was carried out by L'Hoir et al.[7]

We report here a similar experiment using a 17.9 MeV/u ^{79}Br beam from the TASCC cyclotron. Measurements of the distribution in energy and charge state of the exiting ions were made for fifteen energies between 12.1 and 17.5 MeV/u for ions channeled along a <110> direction through a 1 μm Si crystal. In addition, coincidence x-ray data were taken at 13.7, 15.3 and 17.5 MeV/u. A preliminary report[8] of this work appeared earlier.

The principle of the measurement is to use channeling to keep the ions away from rows of atoms, so that the normal charge-exchange processes in close collisions with Si atoms are eliminated. The only close collisions are then with valence (M-shell) electrons, and the probability for dielectronic recombination should be proportional to the average density of valence

electrons along the trajectory. The energy loss of the channeled ions is reduced compared to the loss for ions penetrating a random medium, and ions exiting the crystal with significantly different energies have sampled different regions of the channel. We could therefore study the variation of the capture probability with electron density by selecting windows in the energy-loss spectrum. The results are compared with calculations based on density profiles across the channels obtained from x-ray diffraction measurements.

Since the analysis of these capture measurements is based on the reduction of the energy loss for channeled ions, we discuss in some detail the theoretical description of the energy-loss process. For Si atoms, the K-, L- and M-shells are well separated both in binding energy and in spatial extension and it is natural to consider separate contributions to the stopping as arising from different shells. We discuss the problems of such a separation and compare the resulting predictions with the measurements. A treatment of the random stopping of swift heavy ions, with reference to results obtained in this experiment, was given earlier[9].

In section 2, we give experimental details while section 3 describes analysis of the DR electron capture process. Section 4 compares measurements and calculations of the resonance strength, energy and width, and section 5 details energy-loss measurements. In section 6, the x-ray coincidence data are described and a summary and conclusions are given in section 7.

2. EXPERIMENTAL DETAILS

The experimental layout is shown schematically in Figure 1. A 17.9 MeV/u $^{79}Br^{22+}$ beam from the TASCC facility superconducting cyclotron at Chalk River was stripped/degraded to $^{79}Br^{33+}$ with a series of Al degrader foils. The foils ranged in thickness between 1 mg/cm^2 and 19 mg/cm^2, in steps of 1 mg/cm^2, corresponding to beam energies on target between 17.6 and 12.1 MeV/u. The 90° and 18.5° beam-transport magnets downstream of the degrader foil were used to select a narrow momentum bite of the 33^+ charge-state component of the degraded beam. The beam divergence was controlled by two 0.5 mm apertures, separated by 1.6 m, directly ahead of the scattering chamber.

The cyclotron beam energy was measured upstream of the stripper/degrader foil. Three accurately located time-pickoff detectors, separated by 6.755 m (1 and 2) and 22.540 m (2 and 3), determined the energy of the $^{79}Br^{22+}$ beam to be 17.869 ± 0.027 MeV/u.

A Si crystal, with a <110> axis normal to its surface, was mounted on a 3-axis goniometer in the scattering chamber; the crystal thickness was measured to be 0.99±0.02 μm with a mixed α source (^{239}Pu, ^{241}Am and ^{244}Cm), using the TRIM stopping powers[10]. Before mounting the crystal in the chamber, we removed the native oxide layer on the surface of the crystal by dipping it into a 1% HF solution and then rinsing it in water. To align a <110> axis with the beam direction we used the fact that the ion energy loss is considerably lower for axial and planar channeling than for

penetration in a random direction and searched for directions where a large fraction of the particles had low energy loss.

At each beam energy, we made measurements for both random and aligned orientation of the crystal for two settings of the Q3D magnetic spectrometer field, chosen to select either 31^+, 32^+ and 33^+ ions or 32^+, 33^+ and 34^+ ions in three resistive-wire counters positioned along the focal plane. Each resistive-wire counter had an active length of 35 cm. The dispersion of the Q3D spectrometer is 13 cm/(% $\Delta p/p$) at the middle of the two-metre-long focal plane.

The resistive-wire counters were calibrated at the highest beam energy by removing the crystal and measuring the beam position in each counter for various settings of the magnetic field. For each position x on the counter the radius of curvature ρ in the spectrometer could be calculated from the magnetic field B and the accurately measured beam energy; in subsequent measurements the function $\rho(x)$ was used to determine the energy of the transmitted ions from the magnetic field setting.

Energy-loss spectra for 33^+ and 32^+ (one-electron pickup) ions are shown in Figure 2 for random and aligned orientations at 15.6 MeV/u incident energy. The direct beam had a FWHM of 306 keV, approximately half the width of the peak in random alignment.

A 200 mm^2 intrinsic Ge x-ray detector was mounted in the chamber at 127.5° to the beam direction and approximately 5.3 cm from the Si crystal as shown

in Figure 1. X-rays were recorded in coincidence with 32^+ ions detected in one of the focal plane detectors for incident energies of 13.7 MeV/u, 15.3 MeV/u and 17.6 MeV/u, i.e., below, on and above the KLL resonance, respectively. The incident flux of 33^+ ions was determined from the measured charge-state ratio $32^+/(32^+ + 33^+)$ for channeled ions (see section 3).

The x-ray detector efficiency was measured with a calibrated ^{57}Co source which covered the region of x-ray energies of interest in this experiment. The detector efficiency was observed to change by 60% between 6.4 and 14.4 keV and, since we do not know the magnitude of the effect of the Ge K-absorption edge for the geometry of our detector, we estimate the uncertainty in efficiency to be ~15% in the region between these energies.

A measurement of the charge-state distribution was made for random and <110> alignment at each of the three beam energies where x-ray data were collected. The charge-state measurement at 15.3 MeV/u is shown in Figure 3. We note the very strong reduction of electron capture for channeled ions. Were it not for this effect, it would be very difficult to experimentally identify the DR process directly as an increased yield of ions which captured an electron at the resonance energy.

3. ANALYSIS OF CAPTURE

At the resonance energy for KLL capture, the DR process is responsible for a large fraction of the charge exchange for channeled ions. This can be

seen in Figure 4a where the ratio $32^+/(32^+ + 33^+)$ is shown as a function of beam energy. Figure 4b shows the resonance contribution after the subtraction of a smooth background proportional to E^{-b} with b=2.94 determined empirically by fitting the three lowest-energy points and the highest-energy point.

In this analysis we include only well-channeled particles with low energy loss (i.e., windows I, II and III in Figure 2). To calculate the capture ratio for a group of ions defined by a window in the 33^+ energy-loss spectrum, a corresponding window in the 32^+ spectrum must be identified, which contains ions with the same channeling properties, i.e., which corresponds to the same range of transverse energy. Furthermore, for determination of the dependence of the capture ratio on beam energy, the windows in the energy-loss spectra obtained for different incident-ion energies must also be chosen to correspond to the same range of transverse energy.

For the definition of these windows we have used the peak corresponding to random energy loss as a reference point. At the two extreme energies, 12.1 MeV/u and 17.6 MeV/u, the energy of the 33^+ beam was measured by raising the crystal out of the beam. It was found that the ratio between random energy loss and the leading edge of the channeled energy loss spectrum was the same at these two energies to within 1%. We have therefore defined window boundaries at definite fractions of random energy loss. An alternative procedure would be to define windows by the fraction

of channeled 33^+ ions above the window boundary (i.e., with lower energy loss) in the energy-loss spectrum, and indeed the constancy of this fraction, as a function of bombarding energy, served as a useful check on the consistency of our procedure.

The same fractions of random energy loss were used to define the regions in the 32^+ spectra. The dependence of energy loss on charge state was ignored. For convenience, we may assume that the capture occurs in the middle of the crystal and therefore the energy loss, for a fixed trajectory, should be reduced by about 3% because of the Q^2 dependence of the stopping. However, the random energy loss, which is used as a reference, should also be slightly smaller for exiting 32^+ ions than for 33^+ ions. This difference may be estimated from the observation that the charge-state distribution after the crystal had a small dependence on incident charge state consistent with an exponential approach to equilibrium with a decay length of 1/4 μm. This would give the same energy-loss difference for the random 32^+ and 33^+ ions as for channeled ions, since the random stopping power is about twice as large and the decay length is 1/4 of the crystal thickness. Semi-classical calculations of the cross section for loss of a Br L-shell electron in a collision with a Si nucleus[11] lead to a mean free path for this process of about 1/2 μm (and hence to a decay length of about 1/4 μm), in agreement with the charge-state observations. This estimate may also be applied to set a limit for the correction to the capture ratio for loss of the captured electron in Br^{32+} in collisions with electrons in the channel. The cross section for this process must be smaller by a factor of $\sim 14^2$ and, since the electron

density in the channel is only a few electrons per atom, the correction cannot be larger than ~2%.

In order to obtain information on the variation of the capture probability with electron density, the peak in the energy-loss spectrum for channeled Br^{33+} ions was subdivided into three intervals as shown in Figure 2. As discussed in section 5.2.4, the spread in energy loss results mainly from a variation of the particle trajectory associated with the uniform distribution of the point of impact on the crystal surface, with only a small contribution from straggling in energy loss for a fixed trajectory. Hence larger energy loss should correspond to larger transverse energy, and higher average electron density along the trajectory. For the three selected energy-loss windows, the charge state distributions were analyzed as before (see Figure 4) and the results are shown in Figure 5.

The calculated energy-integrated cross section for dielectronic recombination of He-like ^{79}Br ions[12] is 5.6×10^{-19} eVcm^2. With this value it is possible to deduce the average electron density seen by the channeled ions from the area of the background-corrected distributions shown in Figure 4b and Figure 5. The energy scale must be converted to the equivalent energy (in the ion rest frame) of electrons at rest in the target; the area is then equal to the cross section multiplied by the number of electrons per unit area of the crystal. The results of this analysis are summarized in Table I. The errors include an estimated 4% systematic error (added linearly to the statistical error) resulting from

the method used to determine the non-resonant background. There is a clear variation of derived electron density with energy loss in contrast to earlier measurements[6] (see footnote).

4. COMPARISON OF MEASURED AND CALCULATED ELECTRON DENSITY

Experimentally, the electron density is better known in silicon than in any other material owing to extremely accurate x-ray diffraction measurements. An analytical fit to these measurements, based on the Doyle-Turner representations[13] of x-ray form factors for Si and for Si^{4+} and a Gaussian blob of charge in the bonds, has been made by Scheringer[14] and we shall base our calculations on this model.

Ions with energy loss much smaller than the 'random' value (i.e., for an amorphous target) have been channeled through the crystal. The motion of channeled ions is governed by the transverse potential, U(x,y), i.e., the

---

In a preliminary report on this experiment[8], it was stated that we saw no variation in electron density with energy loss; this resulted from an error in that data analysis which has since been corrected.

crystal potential averaged over the coordinate, z, along the <110> direction. Since the ion is nearly fully stripped, it may be treated as a point charge, Qe, interacting with the electrostatic potential ϕ in the crystal, $U(x,y)=Qe\phi(x,y)$. It is then convenient to define a reduced-transverse-energy, ϵ, of channeled ions as:

$$\epsilon = \frac{p_\perp^{\,2}}{2MQ} + e\phi(x,y) \qquad (1)$$

where $p_\perp$ is the projection of the ion momentum on the transverse (x,y) plane and M is the ion mass.

The calculation of the average electron density along the trajectory of an ion which experiences a given energy loss is based on the following assumptions:

i) The reduced transverse energy, ϵ, is conserved.

ii) The transverse distribution of ion trajectories for fixed ϵ is uniform in the allowed area, corresponding to a statistical equilibrium for transverse motion in the potential U(x,y).

iii) The energy loss ΔE is an increasing function of ϵ.

The first assumption should be quite accurate for our case. In particular, the average increase in reduced transverse energy resulting

from multiple scattering due to electronic collisions may be estimated from the energy loss,

$$\langle \Delta\epsilon \rangle = \Delta E \, \frac{m}{2M} \, \frac{1}{Q} \tag{2}$$

where m is the electron mass. In the middle of the crystal, $\langle \Delta\epsilon \rangle$ is half this amount which in the present case is negligible, $\langle \Delta\epsilon \rangle/2 \simeq 0.1$ eV. Note, however, that if the crystal thickness is increased by an order of magnitude as in the work by Andriamonje et al.[6], this correction becomes significant. The validity of assumptions ii) and iii) is discussed in sections 4.3 and 5, respectively.

4.1 Distribution in ϵ

It is convenient to discuss the integrated distribution

$$G(\epsilon) = \int_0^{\epsilon} d\epsilon' \, g(\epsilon') \tag{3}$$

where $g(\epsilon')$ is the distribution in transverse energy. If the beam is incident parallel to the crystal axis, $G(\epsilon)$ is simply the normalized area function

$$G_o(\epsilon) = A(\epsilon)/A_o \tag{4}$$

i.e., the fraction of the transverse plane available for the motion of particles with reduced transverse energy ϵ. This function is shown in Figure 6.

The collimation of the incident beam corresponds to a distribution f in ϵ and, taking this into account, we obtain

$$G(\epsilon) = \int_0^{\epsilon} d\epsilon' \; f(\epsilon') \; G_0 \; (\epsilon-\epsilon'). \tag{5}$$

For large values of ϵ, where $G_0(\epsilon-\epsilon')$ is approximately linear over the range of $f(\epsilon')$, we obtain

$$G(\epsilon) \simeq G_0 \; (\epsilon - \langle\epsilon'\rangle) \tag{6}$$

$$\text{with } \langle\epsilon'\rangle = \int_0^{\infty} d\epsilon' \epsilon' f(\epsilon')$$

i.e., the function G is just shifted by the average reduced transverse energy of the incident beam. With the collimation used in this experiment, we have $\langle\epsilon'\rangle$ = 1.24 eV at 15.6 MeV/u. The modified function $G(\epsilon)$ is shown as a solid line in Figure 6.

We now use assumption iii) above to calculate the available area for ions in the three windows on the energy-loss spectra (see Figure 2). Via the modified $G(\epsilon)$ curve each window boundary, represented by the fraction of

ions with energy loss lover than that boundary, may be associated with a particular transverse energy. The function $G_o(\epsilon)$ then gives the corresponding available area of the transverse plane as illustrated in Figure 6. The increase in available area caused by the angular spread of the beam is clearly a significant correction.

4.2 Electron Density

The calculated average electron density in a Si<110> channel as a function of the available area in the transverse plane, $x = A(\epsilon)/A_o$, is shown in Figure 7. The solid curve with 0.56 electrons in each bond corresponds to the best fit to the x-ray diffraction data[14] while the dashed curve gives the atomic charge density without correction for bonding. The average density of valence electrons, $\bar{\rho}$ is close to $\bar{\rho} = 1+3x$ electrons/atom and this is a useful approximation. The corresponding approximation for the local density at the boundary of the area $A(\epsilon)$ is $\rho = 1+6x$. The steep rise for $x > 0.8$ is due to L-electrons.

The intervals in x, derived from Figure 6, are given by dashed lines. For the lowest window in ϵ, the measured density of 1.96±0.12 electrons/atom is in very good agreement with the calculation. For the two higher windows, the experimental values of 3.11±0.14 and 3.76±0.22 are ~10-15% higher than the calculated values, i.e., only slighly outside our estimated uncertainties.

For this comparison we have assumed that resonant electron capture is a local process and, hence, the capture probability is proportional to the local electron density averaged along the projectile trajectory. The impact-parameter dependence may be estimated from the angular momenta involved and conservation of angular momentum restricts the l-values for the electron to be captured to $l \leq 2$. The largest value corresponds to a classical impact parameter b = 0.1 Å which is small on the scale of the variation of ρ. Hence there seems to be no reason to suspect an important correction for non-locality as has been suggested by Andriamonje et al.[6].

4.3 Spatial Average

The assumption of a uniform distribution of ion trajectories in the available transverse area, which corresponds to a statistical equilibrium for two-dimensional motion, may be questioned for such a thin crystal (1 μm). In the middle of the channel, the potential is nearly axially symmetric and angular momentum along the axis is approximately conserved. Hence, establishment of full two-dimensional equilibrium requires each channeled trajectory to undergo many oscillations.

Consider for simplicity a harmonic potential U(x,y) corresponding to the average valence electron density of 4 electrons/atom. The oscillation frequency, ω, for the transverse motion of an ion with charge Qe may, through Poisson's equation, be related to the plasma frequency in silicon, ω_{pl} = 16.6 eV/$\hbar$ by:

$$\Delta U = 4\pi\rho e^2 Q = 2\, M\omega^2 \qquad (7)$$

leading to $\omega = (Qm/2M)^{1/2}\ \omega_{pl}$.

The number of oscillations during the time spent traversing the crystal (T=1 μm/v, where v is the ion velocity) is then close to unity and for the lower density in the <110> channel the ions will perform less than one full oscillation.

Nevertheless, estimates based on the assumption of a uniform distribution in two dimensions should be reasonable. As seen in Figure 6, the electron density is nearly linear in the square of the displacement from the channel centre and, for a harmonic oscillator, the average of the square of this distance is independent of the angular momentum for fixed particle energy. Thus, for example, the average square displacement is the same in one- and two-dimensional statistical equilibrium since the average potential energy is half the total energy in both cases.

4.4 Resonance Energy and Width

The resonance condition for KLL capture of a free electron with velocity v_e by an ion with velocity v may be expressed as energy conservation in the ion frame,

$$\tfrac{1}{2}m(\bar{v}_e-\bar{v})^2 = E_K-2E_L \qquad (8)$$

where E_K and E_L are the K- and L-shell binding energies.

The right hand side of Eq. (8) can be obtained from a purely atomic calculation since at the small distances of binding, the screening by electrons in the solid can be neglected. A number of final states with slightly different binding energy contribute and the average, weighted by the partial capture cross section, becomes 8.50 keV [12].

The main term on the left hand side of Eq. (8) is $1/2mv^2$ and hence Er=8.50 keV is a first estimate of the resonance energy; modifications we move to the right hand side as corrections to E_r. We first note that relativistic corrections to the kinetic energy are less than 1% so we may use the non-relativistic expression for calculation of corrections. After averaging over directions of v_e we obtain as the first correction to E_r, $-\langle 1/2mv_e^2 \rangle$. For a Fermi gas the average kinetic energy is 3/5 of the Fermi energy, which is given by

$$E_F = (3\pi^2 \rho_e a_0^3)^{2/3} \qquad (9)$$

in units of a Rydberg, $e^2/2a_0$=13.6 eV, where a_0=0.529 Å is the Bohr radius. With the electron density corresponding to window I (see Table I), the correction to E_r from kinetic energy of the captured electron becomes -5 eV.

Is there a corresponding correction for potential energy? If the collision with the ion is viewed in the laboratory frame, the electron moves only a very small distance of order $b_0 < 0.1$ Å before capture (see Eq. (18)), and hence we can neglect the influence of the lattice potential [Note, that a significant correction for potential energy was erroneously included by Pitharke, et al.[15)]]. However, there is another potential-energy correction which can be significant.

The scattering of target electrons on the ion builds up a polarization potential which repels the electron to be captured and reduces the energy release (left hand side of Eq. (8)). For a uniform Fermi gas in the high-velocity limit, the magnitude of this potential energy at the position of the ion may be written[16)] as [The expression (4.27) in ref. (16) for the self energy of the ion should be multiplied by $2/z_1 e$ to obtain the induced electrostatic potential at the position of the ion.]:

$$V = \frac{\pi}{2} \frac{v_0}{v} Q \hbar\omega_{pl}, \tag{10}$$

where v_0 is the Bohr velocity, Qe the ion charge and $\hbar\omega_{pl}$ the plasmon energy, which in Rydberg units is given by

$$\hbar\omega_{pl} = (16\pi \rho_e a_0^3)^{1/2}. \tag{11}$$

The potential builds up over distances from the ion up to v/ω_{pl}, which for our case is tens of Ångstroms. Hence, for the contribution from valence

electrons we may use Eq. (10) with the plasmon energy in Si, $\hbar\omega_{pl}$=17 eV, which leads to V=35 eV and a positive correction of this magnitude to E_r.

Since the polarization potential is not very local, the contribution from L electrons should also be considered. For a simple estimate, we may again use the formula (10) for a homogeneous electron gas. The proportionality of V to ω_{pl} results from a combination of a proportionality to electron density, i.e., to ω_{pl}^2 according to Eq. (11), and a proportionality to the reciprocal response frequency ω_{pl}^{-1}. For the L electrons, the average density is higher by a factor of two compared to M electrons, but the response frequency is higher by more than an order of magnitude (see Table 1). Hence the contribution from L electrons cannot increase the polarization potential by more than about 15%.

The combined correction to E_r will then be of order 35 eV, leading to a predicted resonance energy of E_r=8.54 keV. For the interval I, the centroid of the resonance peak shown in Figure 5 is 8.50 ± 0.02 keV, in reasonable agreement with the prediction; the uncertainty on the resonance centroid includes uncertainty on the determination of the centroid of the distribution and on the energy calibration of the Q3D spectrometer.

The width of the resonance, resulting from the motion of captured electron results from the term $-2v_e.v$ in equation 8 and can be expressed as

$$\Delta E_{FWHM}/E_r = 2(2E_f/E_r)^{1/2} \qquad (12)$$

The measured resonance widths for regions I, II and III and the predictions, based on Eq. (12) with the measured electron densities are summarized in Table I. Good agreement (~10%) is obtained considering the fact that the electron density in a channel varies considerably with the z coordinate.

5. ENERGY LOSS

The analysis of the experiment is based on the measurement of energy loss and it is therefore important to understand the ΔE-spectra in Figure 2. We first briefly summarize the discussion in ref. [9] of the energy loss and straggling for random incidence.

5.1 Random Energy Loss

For particles with charge Qe and high but still non-relativistic velocity v, the stopping is approximately given by

$$\frac{dE}{dx} = \frac{4\pi\ Q^2\ e^4}{mv^2}\ \rho L_e\,, \tag{13}$$

where ρ is the average electron density, $\rho = NZ_2$, and N is the atomic density. The stopping logarithm may be written as:

$$L_e \simeq \log \frac{b_{max}}{b_{min}}\,, \tag{14}$$

where b_{max} and b_{min} are effective limits in the integration over impact parameters b of the energy transfer to electrons, which for small scattering angles is proportional to b^{-2}. Such a classical description of electron-ion collisions is permitted when Bohr's parameter κ is larger than unity,

$$\kappa = 2Q\ v_o/v, \tag{15}$$

where v_o is the Bohr velocity. For Br^{33+} at 17.6 MeV/u we have κ=2.5.

In distant collisions, an atom responds like a collection of harmonic oscillators. For a single oscillator with frequency ω, the effective upper cut-off in b, due to adiabaticity of the interaction, is given by

$$b_{max} = 1.123\ v/\omega. \tag{16}$$

For an atom, b_{max} is given by Eq. (13) with a weighted average frequency.

$$\log(\omega) = Z_2^{-1} \sum_i f_i \log(\omega_i), \tag{17}$$

where f_i are dipole oscillator strengths fulfilling the sum rule $\sum_i f_i = Z_2$. The energy $I = \hbar\omega$ is denoted the I-value.

In the classical regime, $\kappa>1$, the effective lower limit in the integration over b corresponds to a scattering angle of $\pi/2$ in the relative ion-electron motion, and the impact parameter is given by

$$b_{min} = b_0/2 = Qe^2/mv^2. \qquad (18)$$

The main correction to this description is the so-called Barkas effect, which may be explained as an effect of dynamic (adiabatic) screening of the interaction at large electron-ion distances. For the present experiment, the correction is ~5% and with the above description the measured stopping is then reproduced within a few per cent (Table I of Ref. 9).

The straggling in energy loss was shown in Ref. [9] to have about equal contributions from fluctuations in ion charge (charge-exchange straggling) and from fluctuations in the large-energy transfers in collision with electrons (Bohr straggling). Furthermore, the calculated width of the random energy-loss distribution was in good agreement with the measured width.

5.2 Channeled Energy Loss

5.2.1 Separation of Shells

For channeled ions, the theoretical treatment of energy loss is much more complicated, because of the imposed selection of impact parameters with

atoms. Both the spatial distribution of the electrons and the frequency distribution of the dipole oscillator strengths f_i become important.

A reasonable description of the stopping may be obtained by the customary separation into contributions from different electron shells. For Si there are three shells, the K-, L- and M-shells. While the K- and L-shells are localized near atomic positions, the M-electrons are delocalized in the solid and form the valence band. The binding energies differ by about an order of magnitude and are of order 10^3, 10^2, and 10 eV, respectively.

There are two main complications in this description, the Pauli principle and collective effects. For the first we may refer to the calculation by Dehmer et al.[18] in the independent electron model with Herman-Skillman wave functions. The Pauli principle blocks transitions to filled states and transfers oscillator strength from lower to higher shells. Without this effect, the total oscillator strength for a shell would be equal to the number of electrons it contains. In Si, the main effect is a transfer from the K-shell to the filled L-shell (Figure 7 of Ref. [18]) of about 0.5, as given in Table II. The I-values in the third column of Table II are estimated from Figure 8 of Ref. [18], and with these values we reproduce closely the atomic I-value given in Ref. [18], I=131.5 eV.

This I-value is much smaller than the empirical value[17] of I=174.5 eV. The main reason is that the calculation ignores collective effects which,

according to the estimate by Lindhard and Scharff[19], should increase the characteristic response frequencies by an average factor of about $\sqrt{2}$. Semi-empirical estimates of shell I-values are given in the fourth column of Table II. Because of the large differences between the shells in both spatial extension and binding, the collective effects are mainly confined to interactions between electrons in one shell. For the K-shell, this effect should be small and, for the M-shell, the increase to about 17 eV is known empirically from the observed plasma frequency in Si. The I-value for the L-shell is then determined from the total I-value through Eq. (17) and the increase by a factor ~1.3 from the independent-electron result is not too far from $\sqrt{2}$. The effective I-value for the L-shell is an important parameter for the following estimates of energy loss for channeled ions.

5.2.2 Energy Loss to K- and L-shells

We consider now the energy loss for well channeled $^{79}Br^{33+}$ ions at 15.6 MeV/u. For both the K- and L-shells, the ion trajectories are well outside the shell radius, so only energy loss in distant collisions remains. We may then estimate the energy loss from the result for a classical harmonic oscillator with frequency $\omega=I/\hbar$[20], where I is the shell I-value. At impact parameters comparable to the adiabatic distance, $b_{ad}=v/\omega$, the energy loss ΔE is reduced compared to the energy transfer ΔE_{free} to a free electron at the same impact parameter b because the electron adjusts adiabatically to the slowly-varying external field. The reduction factor is approximately[20,21]

$$R(\xi) = \xi^2 \, [K_0^2 \, (\xi) + K_1^2 \, (\xi)], \tag{19}$$

where $\xi = b/b_{ad}$, and K_0 and K_1 are modified Bessel functions[22].

For the two shells, the adiabatic distances are $b_{ad}^K = 0.11$ Å and $b_{ad}^L = 1.16$ Å, and for a trajectory in the middle of a <110> channel the distance to the nearest strings is about 2 Å (see Figure 8). The factor $R(\xi)$ is about 0.5 for $\xi \sim 1$ and decreases as $\exp(-2\xi)$ for large ξ. The energy loss to the K-shell, which is ~6% of the total loss for random stopping, is therefore completely negligible for channeled ions.

The energy loss to the L-shell is also strongly reduced by adiabaticity and we shall try to estimate the magnitude of this loss. The minimum contribution from the L-shells, ΔE_{min}^L, is obtained for an ion moving along the centre of a <110> channel. As seen in Figure 8, the ion is then surrounded by 6 strings, each at a distance of $r_{ch} \simeq 2$ Å. Adiabaticity makes the energy loss negligible to L-electrons in strings further away.

Each time the ion moves through a <110> lattice spacing, d = 3.84 Å, it collides with 6x8 = 48 L-electrons at impact parameter $b \simeq r_{ch}$. The small transfer of oscillator strength from the K-shell (see Table II) in effect increases this number to 51 electrons. The energy loss to free electrons would be

$$\Delta E_{free} = n \left[\frac{b_0}{b}\right]^2 \left[\frac{1}{2} mv^2\right] \left[\frac{t}{d}\right] \tag{20}$$

which with n=51, b=r_{ch} and t = 1 μm gives ΔE_{free} = 0.88 MeV. The adiabaticity parameter is ξ = 1.72 and the reduction factor R(ξ) is then 0.20, leading to ΔE^{L}_{min} = 0.18 MeV.

For comparison with the experimental spectrum in Figure 2, we select the upper boundary of window I, corresponding to a measured energy loss of 0.41 times random, or ΔE_{exp} = 1.83 MeV. According to Figure 6, the channeled ions with this energy loss have a transverse energy corresponding to an allowed area $A(\epsilon)/A_o$ = 0.19. A circle with this area and radius Δr=0.79 Å is illustrated in Figure 8, and an average of the energy loss to L-electrons must be estimated over this circle.

First we estimate the average of ΔE_{free} given by Equation (20). For a displacement, r, of the ion from the centre, the square of the distance to one of the six surrounding strings becomes $b^2 = r_{ch}^2 + r^2 - 2r_{ch} r \cos\theta$, where θ is the angle between the displacement and the direction towards the string. The averaging of b^{-2} over θ and over r can be carried out analytically and we obtain

$$\langle b^{-2} \rangle = \frac{1}{\Delta r^2} \int_0^{\Delta r^2} dr^2 \frac{1}{2\pi} \int_0^{2\pi} d\theta \, (r_{ch}^2 + r^2 - 2r_{ch} \, r \cos\theta)^{-1}$$

$$= - \Delta r^{-2} \log (1-\Delta r^2/r_{ch}^2) \qquad (21)$$

For Δr = 0.79 Å, we obtain $\langle b^{-2} \rangle = 1.09 \, r_{ch}^{-2}$ and hence the average of ΔE_{free} is 9% larger than the minimum value.

However, the adiabatic reduction factor $R(\xi)$ should be included. It turns out that for the range of ξ-values in question, $R(\xi)$ can be approximated well by $R(\xi) \propto \xi^{-2}$. An average of $R(\xi)\Delta E_{free}$ analogous to Equation (21) can then be carried out analytically and we obtain $\Delta E^{L} \simeq 1.4\ \Delta E^{L}_{min} = 0.25$ MeV.

5.2.3 Energy Loss to M-shell

According to Eqs. (13), (14), (16) and (18) with $\hbar\omega$ = 17 eV, the energy loss in a 1 μm crystal for $^{79}Br^{33+}$ at 15.6 MeV/u to the valence electrons is 2.25 MeV for a uniform flux distribution, and this is therefore the limit for high transverse energy. In a <110> channel, the density of valence electrons is lower than average and hence the energy loss is lower. The average electron density, as a function of the fraction x of the transverse area available, is shown in Figure 7 and, as discussed before, the dependence may be approximated by $\bar{\rho}(x) = 1 + 3x$ (electrons/atom), corresponding to the density variation $\rho(x) = 1 + 6x$.

We use this approximation to estimate the reduction for a trajectory in the centre of a <110> channel. The area of a <110> channel is $\pi r_o^2 = 2\,(Nd)^{-1}$, since along the <110> direction there are two strings associated with each channel. The corresponding value of r_o is 1.82 Å. If we assume the M-electron density to be in effect uniform outside this radius, the stopping logarithm is modified to

$$L_e^M = \log \frac{1.123\ \hbar v/I_M}{r_o} + \int_0^{r_o^2} \frac{db^2}{8(b^2+b_o^2/4)} \cdot \rho \frac{b^2}{r_o^2} \qquad (22)$$

and the reduction in the logarithm becomes

$$\delta L_e^M = -\frac{3}{4}\left[\log \frac{2r_o}{b_o} - 1\right] \qquad (23)$$

which for 15.6 MeV/u $^{79}Br^{33+}$ gives $\delta L_e^M = -2.38$ and $\Delta E^M_{min} \simeq 1.46$ MeV. This value is not very sensitive to the approximation for $\rho(x)$ and the same result is obtained with a linear dependence of ρ on $r \propto x^{1/2}$, as applied by L'Hoir et al.[7]. If we assume L_e^M to increase linearly with the available area towards the random value, we obtain for $A(\epsilon)/A_o = 0.19$ a value $\Delta E^M \simeq 1.61$ MeV. Adding the contribution from the L-shell, we obtain $\Delta E \simeq 1.86$ MeV, in almost exact agreement with the experimental value of $\Delta E_{exp} = 1.83$ MeV.

We note that the inclusion of the energy loss to L-electrons is important for this agreement and that this contribution becomes even more important at higher velocities, where the adiabaticity parameter is smaller. In the analysis of similar experiments with 27 MeV/u Xe ions, L'Hoir et al.[7] disregarded the energy loss to L-electrons. The authors of ref. [7] argued that energy loss to L-electrons was unimportant for well channeled ions because the impact parameters with Si atoms are large compared with the value at which the classical energy transfer to an electron (Eq. (20)

with n=t/d=1) equals the L-shell binding energy (E_L=112 eV). As discussed by Bohr[20], this argument is incorrect. The classical formula gives the average energy transfer correctly at large impact parameters, also when it is small compared with the minimum energy quantum which can be absorbed by the system. The correct cut-off of energy transfers is at impact parameters b ~ $\hbar v/I$ due to adiabaticity, as discussed above.

5.2.4 Energy Loss Distribution

The two dominant contributions to straggling in random energy loss (i.e. charge exchange and close collisions with electrons) are both strongly reduced for channeled ions. The charge state is frozen and the electron density seen by the ions is reduced by nearly an order of magnitude. Hence, the width of the energy-loss distribution is completely dominated by the variation in channeling trajectories associated with the uniform distribution of the point of ion impact on the crystal surface. Our assumption that ΔE is a function of transverse energy should be reasonable. We now examine whether the width of the observed ΔE-spectrum (Figure 2) is consistent with this assumption.

We use the random energy loss windows defined in Figure 2. With the corrections illustrated in Figure 6, the energy losses corresponding to the boundaries of the windows are associated with allowed areas for transverse motion of channeled ions, and analytical estimates analogous to those discussed above can be carried out. For the intervals I and II,

these estimates give widths of ~0.3 MeV, with equal contributions from the L- and M-shells to the change in ΔE, in good accord with the experiment. It should be noted, however, that the assumption in these estimates of a circular geometry to the allowed area becomes increasingly unrealistic for increasing transverse energy.

At high transverse energy, the energy loss increases rapidly, mainly due to the energy loss to L-electrons which for random incidence is more than half the total energy loss. The spectrum in Figure 2 stretches to energy losses considerably larger than for random incidence. This can be understood as an effect of planar blocking: ions with high transverse energy are incident near a string and are blocked by planes containing the string. Hence they are confined to the shoulder regions (relative to planes) and their flux will be higher near strings than would be the case for random incidence.

6. X-RAY COINCIDENCE DATA

Coincident x-ray spectra for the three $^{79}Br^{33+}$ bombarding energies 13.7, 15.3 and 17.6 MeV/u (i.e., below, on and above the KLL resonance, respectively) are shown in Figure 9. The Br x-rays correspond to well-channelled ions, i.e., to the sum of regions I, II and III in Figure 2a. The spectra have been normalized to the same number of incident 33^+ ions.

Inspection of Figure 9 shows that at 17.5 and 13.7 MeV/u (Figure 9a and 9c, respectively) the Kα line is clearly separated from the L and M radiative electron capture (REC) peaks. At 15.3 MeV/u (Figure 9b) the L-REC and Kα energies coincide and cannot be distinguished experimentally. The three spectra also show that the X-ray yield associated with charge exchange is lower by an order of magnitude above and below the resonance and, thus, that a considerable amount of the background in the $32^+/(32^+ + 33^+)$ ratio (Figure 4a) is from non-radiative capture.

During replay of the x-ray data we also generated 32^+ particle spectra for those ions which were in coincidence with a Br Kα x-ray. The results for the three bombarding energies are shown in Figure 10, again normalized to the same number of incident ions. At 17.6 MeV/u and 13.7 MeV/u the K_α x-rays are associated with poorly channeled ions as can be seen in Figures 10a and 10c while near the peak of the DR resonance, Figure 10b, the majority of the K_α x-rays are associated with well channeled ions.

From the intensities of the lines in the x-ray spectra shown in Figure 9 we can calculate electron densities using the calculated flux of incident ions and the measured efficiency of the x-ray detector. From the intensities of the REC lines in the spectra taken at the three energies we derive electron densities for well-channeled ions along the <110> axis of Si as shown in Table III. The Bethe-Salpeter[23] cross section was used in the calculations and we included the sum of the M-,N- and O-REC calculated cross sections for the lower energy REC line. Inspection of Table III

shows that good agreement is obtained among the derived values of the electron densities but the value is about 30% lower than the electron density value of 2.81 ± 0.17 electrons/atom derived from the charged-particle data.

From the intensities of the K_α x rays at the three energies we can derive a value for the DR capture probabilities. The values obtained are $4.6\pm2.0\times10^{-4}$, $5.4\pm1.1\times10^{-3}$ and $3.0\pm0.6\times10^{-4}$ at 13.7, 15.3 and 17.5 MeV/u respectively. The Kα yield at 15.3 MeV was corrected for L-REC by scaling the M-REC intensity by the ratio of the Bethe-Salpeter[23] L-REC/(M+N+O-REC) cross sections. Comparisons of these numbers with the directly measured capture probabilities shown in Figure 4b shows that at 15.3 MeV/u, the x-ray data is again about 30% lower. In the work of Andriamonje et al[6] the x-ray data also yielded a value about 30% lower than the particle data. However, because of the uncertainties in efficiency calibration, we, like Andriamonje et al., do not ascribe any significance to these differences.

7. SUMMARY

We have measured the KLL, DR resonance in electron capture for He-like $^{79}Br^{33+}$ ions, as an enhancement in the $32^+/(32^++33^+)$ ratio for channeled ions in a thin Si crystal. Through x-ray coincidence measurements below, on and above the KLL resonance it was confirmed that this is associated with resonance enhancement in L-REC when the x-ray energy matches the K_α atomic transition.

Using a calculated DR cross section, we determined that the electron density for well channeled ions along a Si <110> axis is 2.81 ± 0.17 e^-/atom. Through a detailed study of the energy loss of channeled ions, a variation in electron density across the channel was observed which agrees well with predictions based on x-ray diffraction measurements.

An analysis of energy-loss processes showed that the measured spectra can be understood from a separation of contributions to the stopping arising from the K, L and M shells of the Si atoms. Although the M-shell electrons dominate the stopping of well channeled ions, there is a significant contribution from distant collisions with L-shell electrons.

8. ACKNOWLEDGEMENTS

We thank the TASCC facility operating staff for providing a high quality, stable ^{79}Br beam. It is a pleasure to acknowledge NATO support through a collaborative research grant CRG 901025, partial support by the U.S. Department of Energy under Contract W-31-109-ENG-38 and support for travelling by the Danish Natural Science Research Council and from the research centre ACAP funded by the Danish Foundation for Basic Research. We are very grateful to N.R. Badnell for discussions on x-ray distributions in REC and DR.

REFERENCES

1. J.A. Tanis, S.M. Shafroth, J.E. Willis, M. Clark, J. Swenson, E. Strait and J.R. Mowat, Phys. Rev. Lett. 47 (1981) 828.

2. S. Datz, C.R. Vane, P.F. Dittner, J.P. Giese, J. Gomez del Campo, N.L. Jones, H.F. Krause, P.D. Miller, M. Schulz, H. Schöne and T.M. Rosseel, Phys. Rev. Lett. 63 (1989) 742.

3. A. Belkacem, E.P. Kanter, K.E. Rehm, E.M. Bernstein, M.W. Clark, S.M. Ferguson, J.A. Tanis, K.H. Berkner and D. Schneider, Phys. Rev. Lett. 64 (1990) 380.

4. P.F. Dittner, C.R. Vane, H.F. Krause, J. Gomez del Campo, N.L. Jones, P.A. Zeijlmans van Emmichoven, U. Bechthold and S. Datz, Phys. Rev. A45 (1992) 2935.

5. J.U. Andersen, J. Chevallier, G.C. Ball, W.G. Davies, J.S. Forster, J.S. Geiger, J.A. Davies and H. Geissel, Phys. Rev. Lett. 70 (1993) 750.

6. S. Andriamonje, M. Chevallier, C. Cohen, N. Cue, D. Dauvergne, J. Dural, R. Genre, Y. Girard, R. Kirsch, A. L'Hoir, J.C. Poizat, Y. Quéré, J. Remillieux, D. Schmaus and M. Toulemonde, Phys. Lett. A164 (1992) 184.

7. A. L'Hoir, S. Andriamonje, R. Anne, N.V. DeCastro Faria, M. Chevallier, C. Cohen, J. Dural, M.J. Gaillard, R. Genre, M. Hage-Ali, R. Kirsch, B. Farizon-Mazuy, J. Mory, J. Moulin, J.C. Poizat, Y. Quéré, J. Remillieux, D. Schmaus and M. Toulemonde, Nucl. Instr. and Meth. B48 (1990) 145.

8. J.S. Forster, T.K. Alexander, J.U. Andersen, G.C. Ball, J.A. Davies, W.G. Davies, J.S. Geiger, H. Geissel and E.P. Kanter, Rad. Eff. and Defects in Solids 126 (1993) 299.

9. J.U. Andersen, G.C. Ball, J.A. Davies, W.G. Davies, J.S. Forster, J.S. Geiger, H. Geissel and V.A. Ryabov, Nucl. Instr. & Meth. B90 (1994) 104.

10. J.F. Ziegler, J.P. Biersack and U. Littmark, "The Stopping and Range of Ions in Solids" (Pergamon, 1985).

11. J.M. Hansteen, O.M. Johnsen and L. Kochbach, Atomic Data and Nuclear Data Tables 15 (1975) 305.

12. N.R. Badnell and P. Zimmerer, private communication.

13. P.A. Doyle and P.S. Turner, Acta Crystallogr. Sec. A24 (1968) 390.

14. C. Scheringer, Acta Crystallogr. Sec. A36 (1989) 205.

15. J.M. Pitharke, R.h. Ritchie and P.M. Echenique, Phys. Rev. B43 (1991) 62.

16. J. Lindhard, Kgl. Dan. Vid. Selsk. Mat. Fys. Medd. 28 (1954) No. 8.

17. J.F. Janni, Atomic Data and Nucl. Data Tables 27 (1982) 147.

18. J.L. Dehmer, M. Inokuti and R.P. Saxon, Phys. Rev. A12 (1975) 102.

19. J. Lindhard and M. Scharff, Kgl. Dan. Vid. Selsk. Mat. Fys. Medd. 27 (1953) No. 15.

20. N. Bohr, Kgl. Dan. Vid. Selsk. Mat. Fys. Medd. 18 (1948) No. 8.

21. J.D. Jackson, "Classical Electrodynamics", p. 625 (Wiley & Sons 1975, 2nd Edition).

22. M. Abramowitz and I.A. Stegun, Handbook of Mathematical Functions, Dover Publications (New York) 1965.

23. H.A. Bethe and E.E. Salpeter, "Quantum Mechanics of One- and Two-Electron Atoms" (Academic Press, New York, 1957) p. 320-322.

TABLE I

ELECTRON DENSITIES DETERMINED FROM RESONANCE YIELDS AND A COMPARISON OF CALCULATED AND MEASURED RESONANCE WIDTHS

Window	Random energy loss fraction	Channeled[a] Fraction	ρ_e[b] (electrons/ atom)	$\Delta E_{FWHM}/E_r$ (%)	
				Predicted	Measured
I	0.41-0.48	0.07-0.28	1.96±0.12	8.5	8.2 ± 0.5
II	0.48-0.55	0.28-0.57	3.11±0.14	9.9	10.9 ± 0.4
III	0.55-0.62	0.57-0.76	3.76±0.22	10.6	11.8 ± 0.5
I-III	0.41-0.62	0.07-0.76	2.80±0.07	9.6	10.5 ± 0.2

a) Fraction of channeled ions in the region determined by the random energy loss window.

b) 1 electron/atom = 0.05 $e^-/\mathring{A}^3$

TABLE II

Shell	Dipole Oscill. Strength	I-value[a]	I-value[b]
K	1.5	3200 eV	3200 eV
L	8.5	240 eV	310 eV
M	4.0	11 ev	17 eV

a) Estimated from Figure 8 of Ref. [16].

b) Collective effects included (see text).

TABLE III

ELECTRON DENSITIES (e^-/atom) IN THE Si<110> CHANNEL DERIVED FROM REC X-RAY YIELDS ASSUMING THE BETHE-SALPETER CROSS SECTION

E (MeV/u)	L-REC[a)]	(M+N+O)-REC[a)]
17.5	1.94 ± 0.37	2.08 ± 0.41
15.3	[b)]	2.10 ± 0.64
13.7	1.54 ± 0.61	2.24 ± 0.94

a) The errors include an estimated 15% systematic error (added linearly to the statistical error) in the absolute efficiency calibration (see section 2).

b) L-REC and K_α are unresolved at this energy.

FIGURE CAPTIONS

Figure 1 Schematic diagram of the experimental layout for heavy-ion channeling studies at the TASCC facility.

Figure 2 Energy spectra of transmitted 32^+ and 33^+ ions for an incident beam of 15.6 MeV/u $^{79}Br^{33+}$ ions. Spectra for random (----) and <110> alignment (—) are shown as a function of energy loss relative to the beam energy. The regions I, II and III correspond to the regions of energy loss used in determining the ratio $32^+/(32^+ + 33^+)$.

Figure 3 The charge-state distribution for random (□) and <110> alignment (Δ), with no window on the energy-loss spectra, for an incident beam of 15.3 MeV/u $^{79}Br^{33+}$ ions.

Figure 4 (a) The charge-state fraction $32^+/(32^+ + 33^+)$ for ions with energy loss encompassing regions I, II and III in figure 2, plotted as a function of energy at the centre of the crystal for <110> alignment.

(b) Background-subtracted charge-state fraction $32^+/(32^+ + 33^+)$ for the data shown in (a) (see text for details of background subtraction).

Figure 5 The background-subtracted charge-state fraction $32^+/(32^+ + 33^+)$ for the regions in energy loss, shown in figure 2, corresponding to windows I(Δ), II(x), and III(□).

Figure 6 The normalized area function, $G_o(\epsilon)$, as a function of reduced transverse energy, ϵ, (– –). The modified function $G(\epsilon)$ (—) takes into account the increase in transverse energy introduced by the finite collimation used in the experiment. The ··· lines represent values of $G(\epsilon)$ and the corresponding value of $G_o(\epsilon)$ (with the same ϵ) for the boundaries of the energy-loss windows I, II and III in Figure 2.

Figure 7 The calculated average electron density, $\bar{\rho}$, for a Si <110> axis as a function of the available area in the transverse plane, $x = A(\epsilon)/A_o$ (–·–). The correction for 0.56 electrons in each bond is also shown (—). The (--) lines represent the values of x corresponding to the boundaries of regions I, II and III of the energy-loss spectra in Figure 2, including the correction for beam divergence illustrated in Figure 6.

Figure 8 Diagram of the transverse plane for a Si <110> axis showing distances between strings of atoms along the axis. The circle in the centre of the channel indicates the confinement corresponding to the upper end of window I in Figure 2 (i.e., $A(\epsilon)/A_o = 0.19$).

Figure 9 X-ray spectra in coincidence with well-channeled $^{79}Br^{32+}$ ions corresponding to the region encompassed by windows I, II and III in Figure 2 for (a) 17.5 MeV/u, (b) 15.3 MeV/u and (c) 13.7 MeV/u. The spectra have been normalized to the same number of incident $^{79}Br^{33+}$ ions.

Figure 10 Energy-loss spectra for $^{79}Br^{32+}$ ions in coincidence with Br K_α x-rays for incident $^{79}Br^{33+}$ bombarding energies of (a) 17.5 MeV/u, (b) 15.3 MeV/u and (c) 13.7 MeV/u. The spectra have been normalized to the same number of incident $^{79}Br^{33+}$ ions.

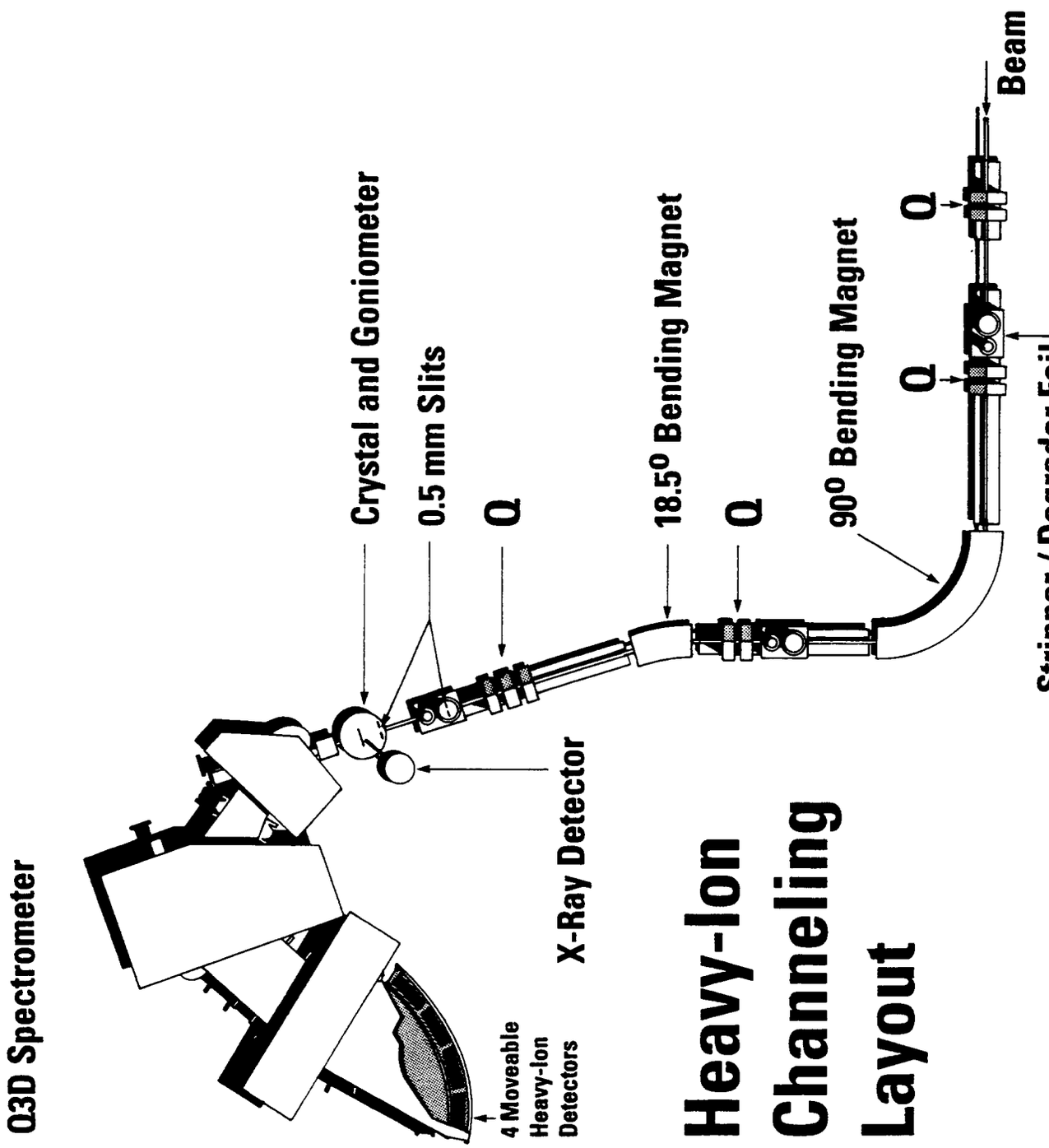
Q3D Spectrometer
4 Moveable Heavy-Ion Detectors
X-Ray Detector
Crystal and Goniometer
0.5 mm Slits
Q
18.5° Bending Magnet
Q
90° Bending Magnet
Q
Q
Beam
Stripper / Degrader Foil
Heavy-Ion Channeling Layout

Fig. 1

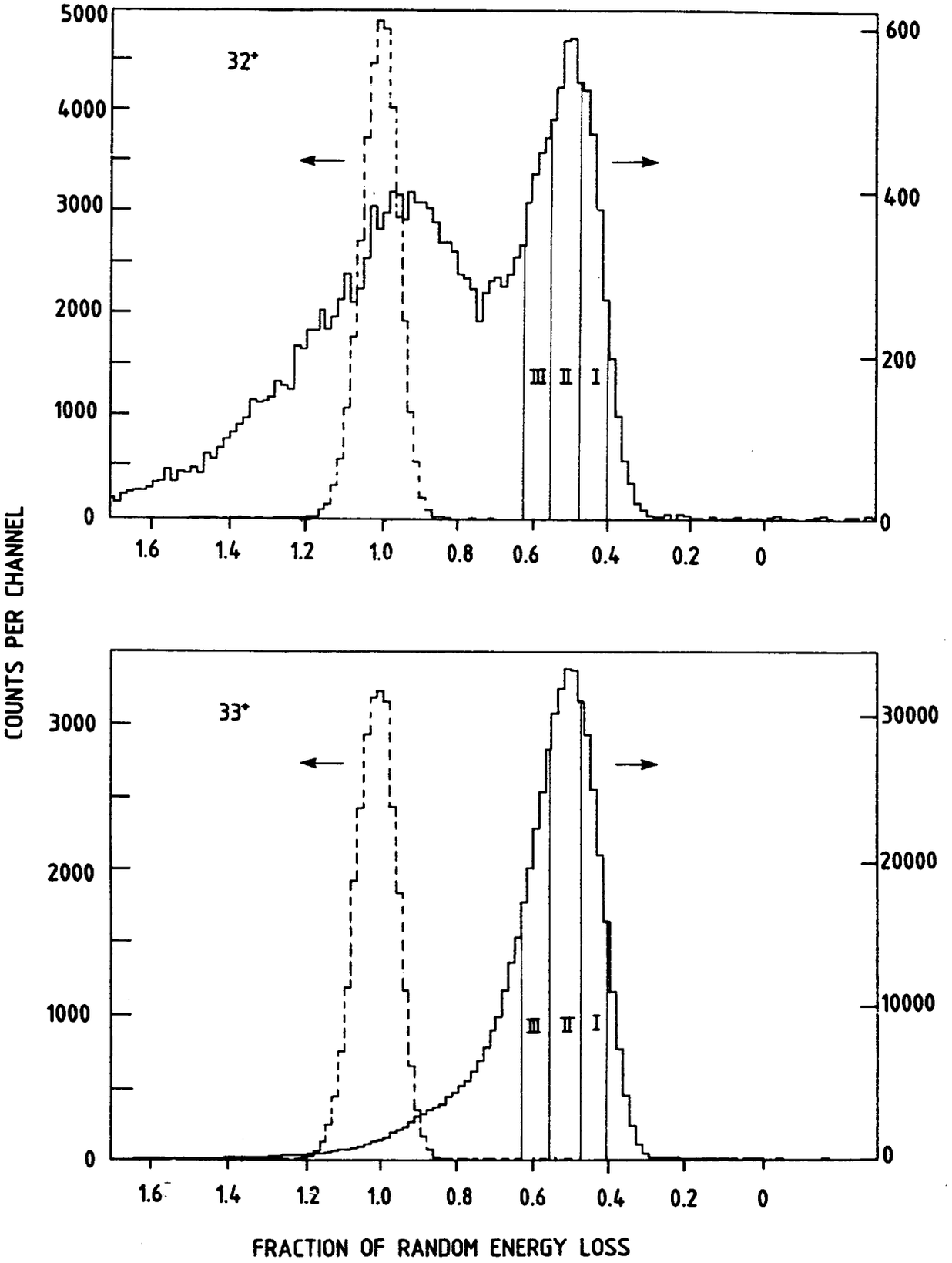
32+
33+
III
II
I
COUNTS PER CHANNEL
FRACTION OF RANDOM ENERGY LOSS
5000
4000
3000
2000
1000
0
600
400
200
30000
20000
10000
1.6
1.4
1.2
1.0
0.8
0.6
0.4
0.2
0

Fig. 2

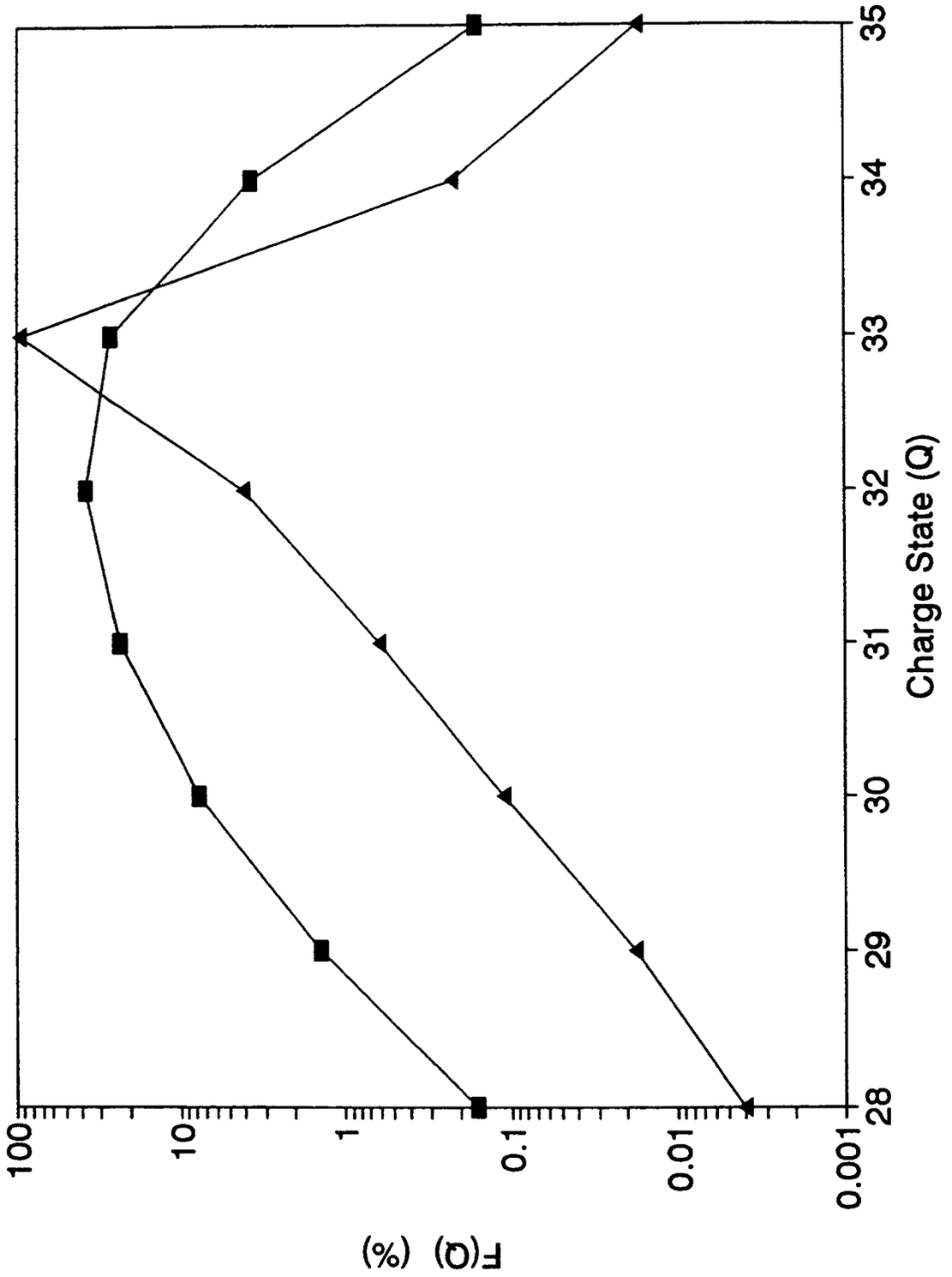

Fig. 3

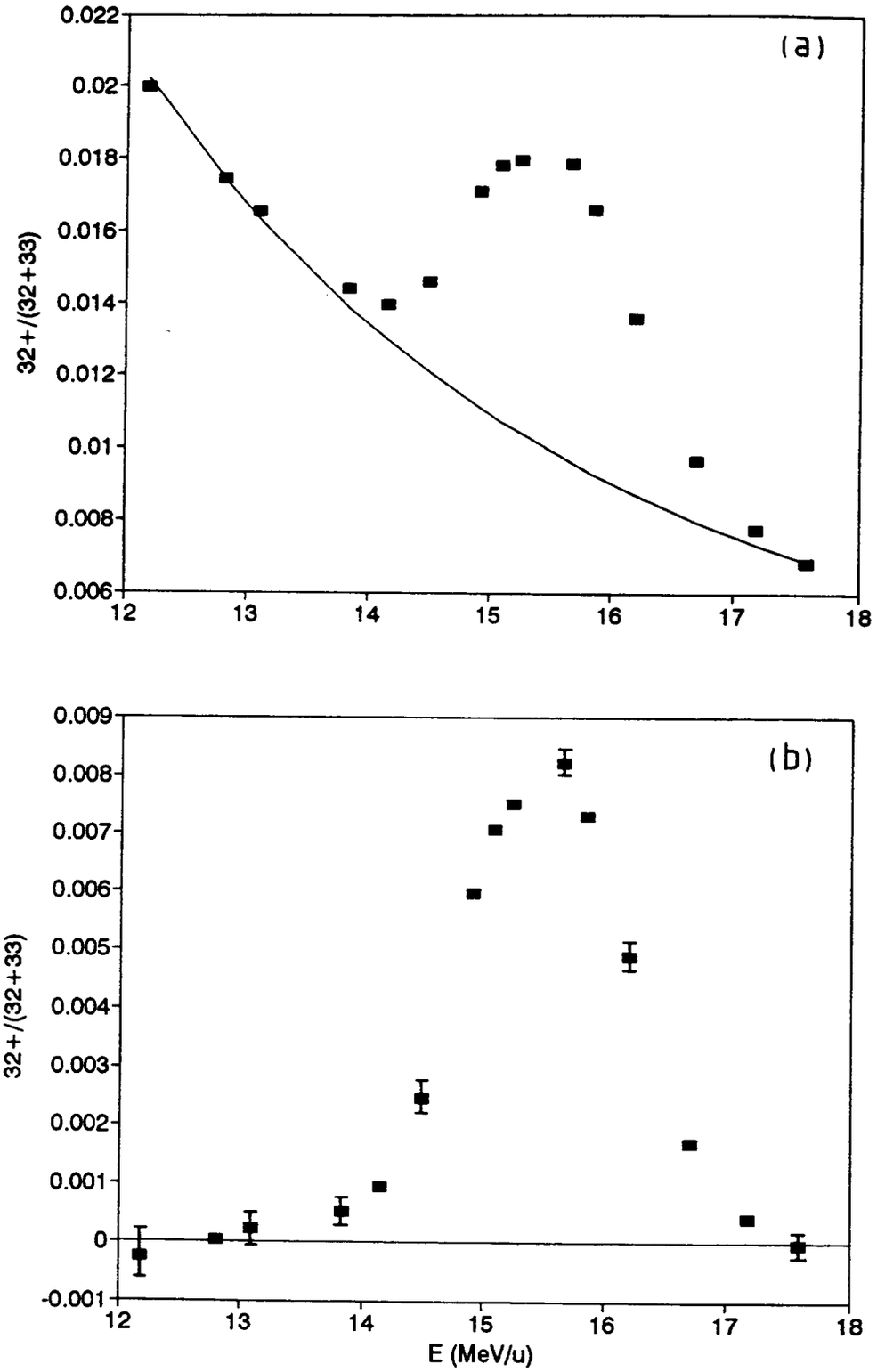
(a)
(b)
32+/(32+33)
E (MeV/u)
0.022
0.02
0.018
0.016
0.014
0.012
0.01
0.008
0.006
0.009
0.007
0.005
0.004
0.003
0.002
0.001
0
-0.001
12
13
14
15
16
17
18

Fig. 4

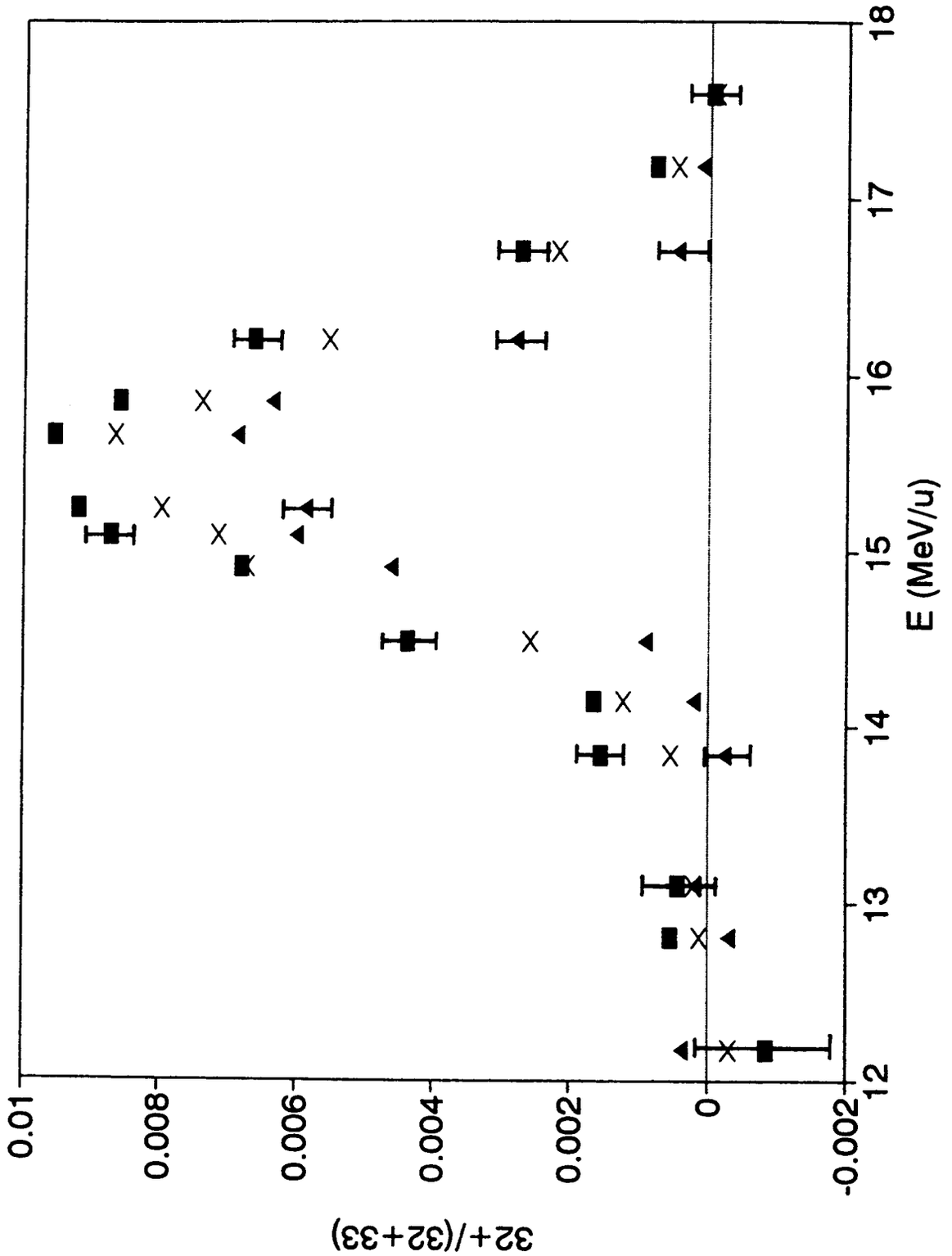

Fig. 5

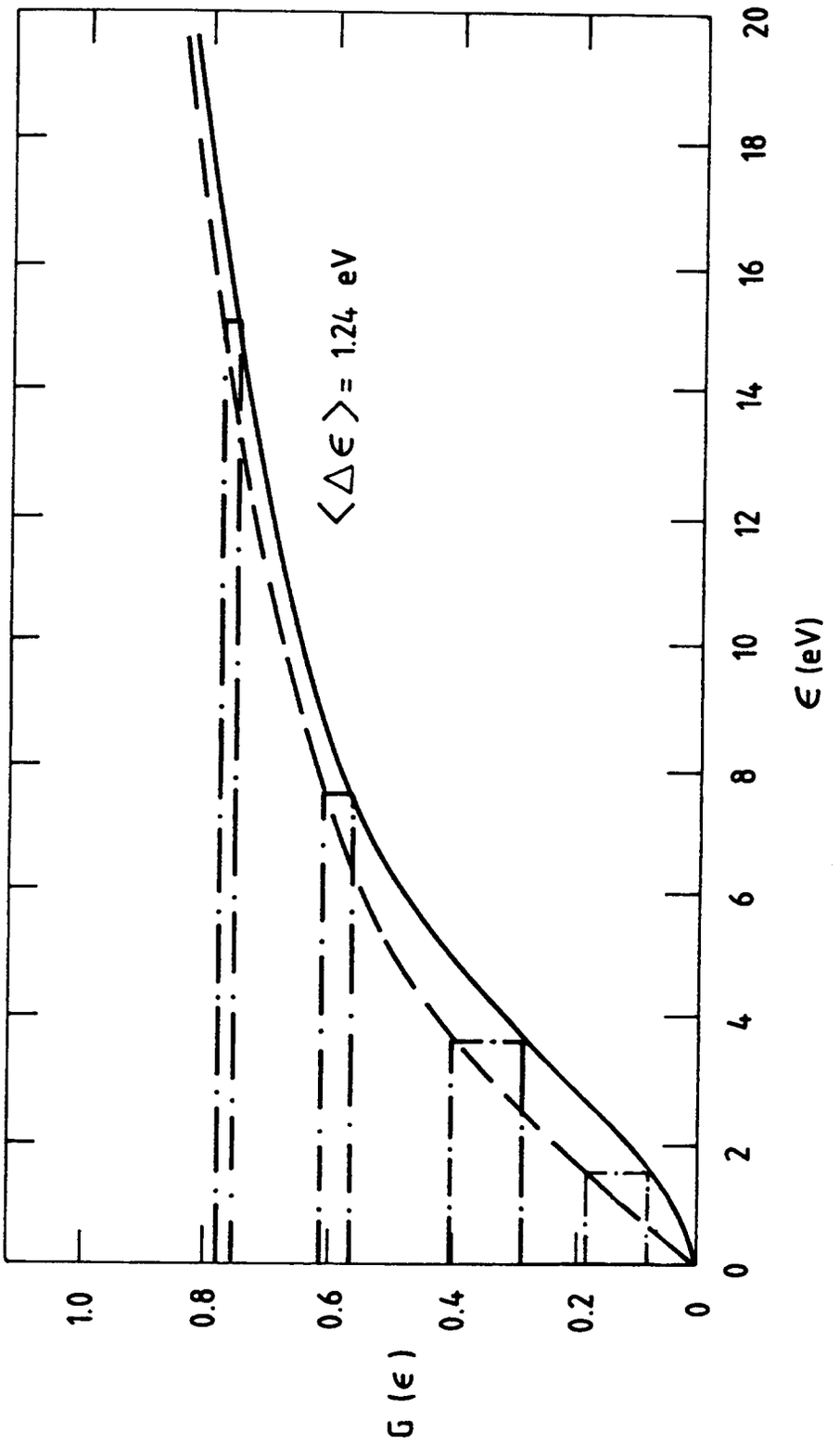

Fig. 6

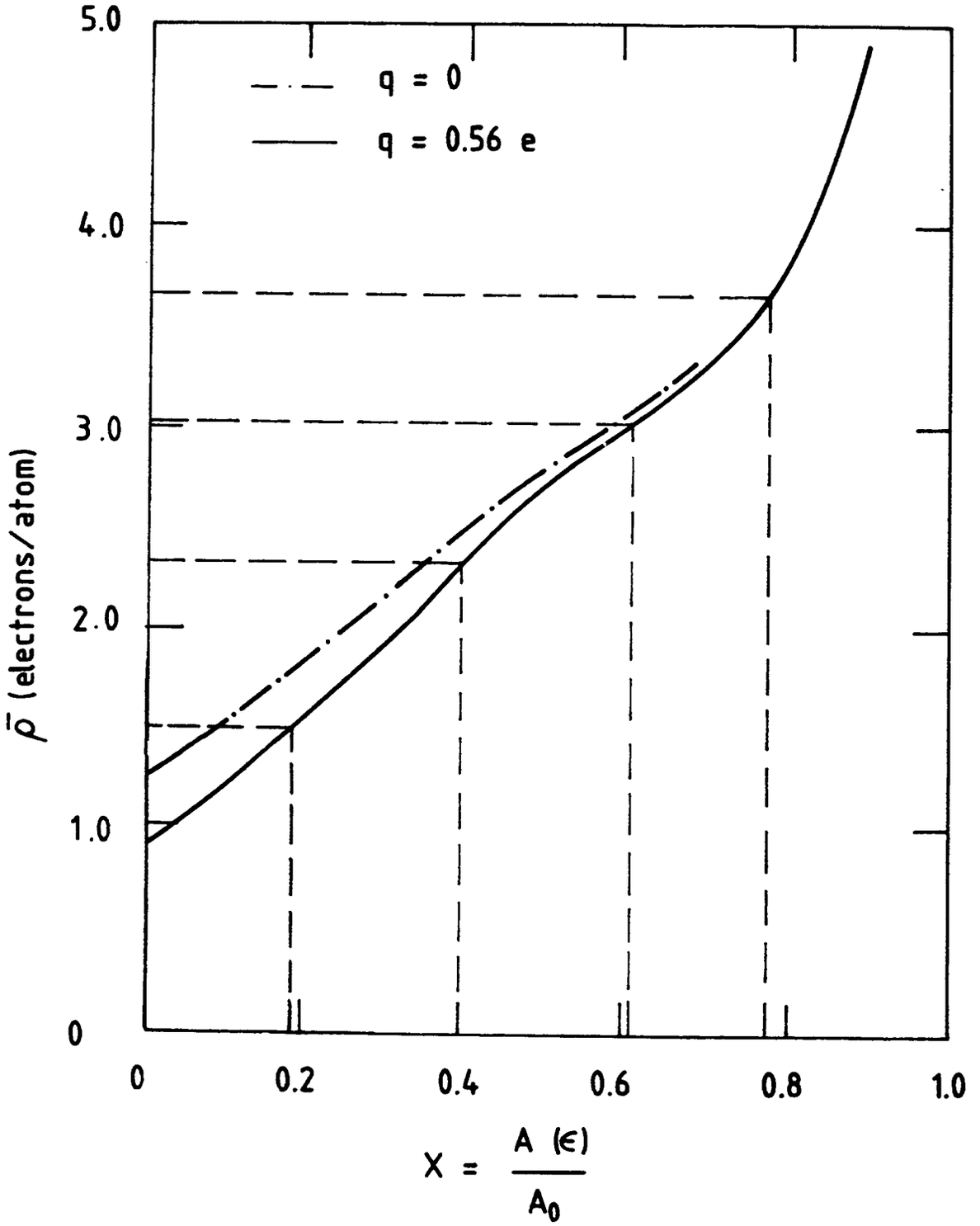
5.0
4.0
3.0
2.0
1.0
0
q = 0
q = 0.56 e
$\bar{\rho}$ (electrons/atom)
0
0.2
0.4
0.6
0.8
1.0
$X = \frac{A(\epsilon)}{A_0}$

Fig. 7

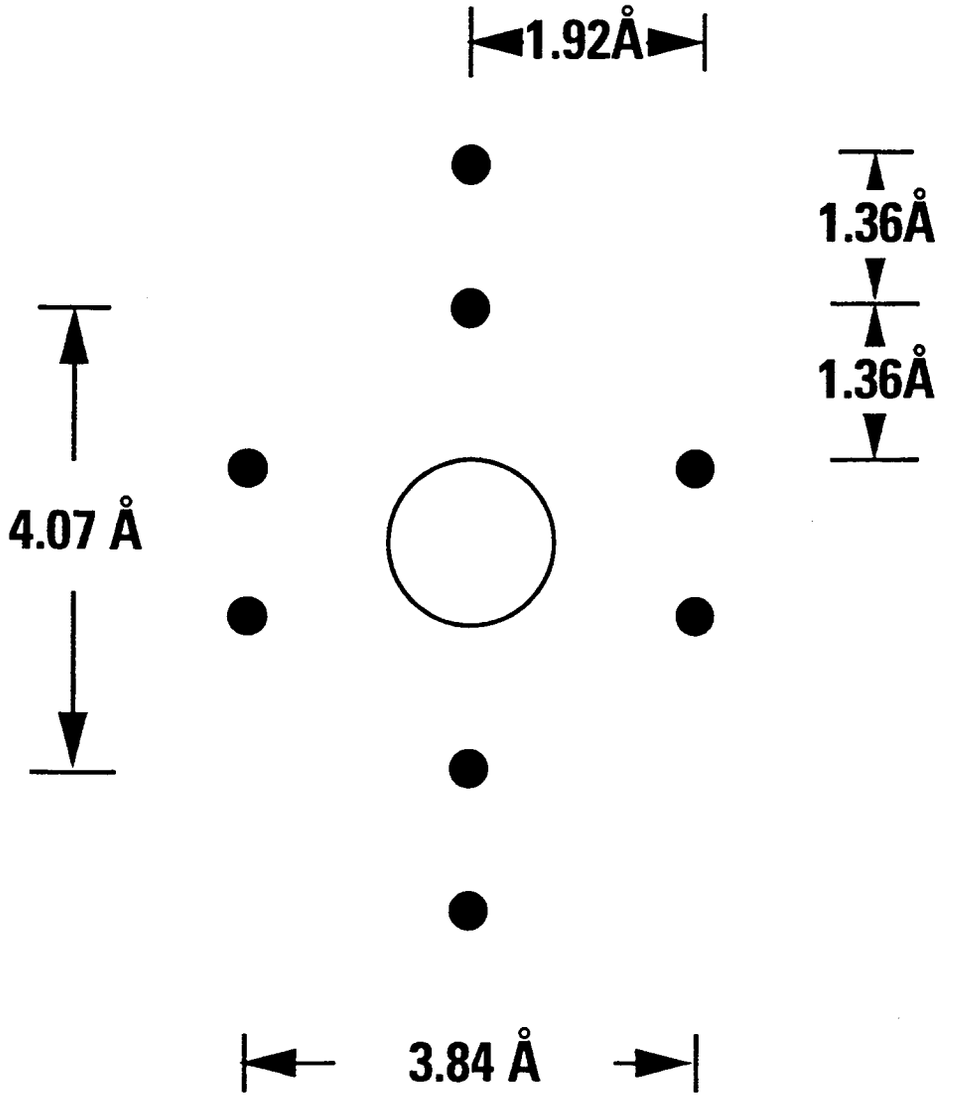

Si <110>

Fig. 8

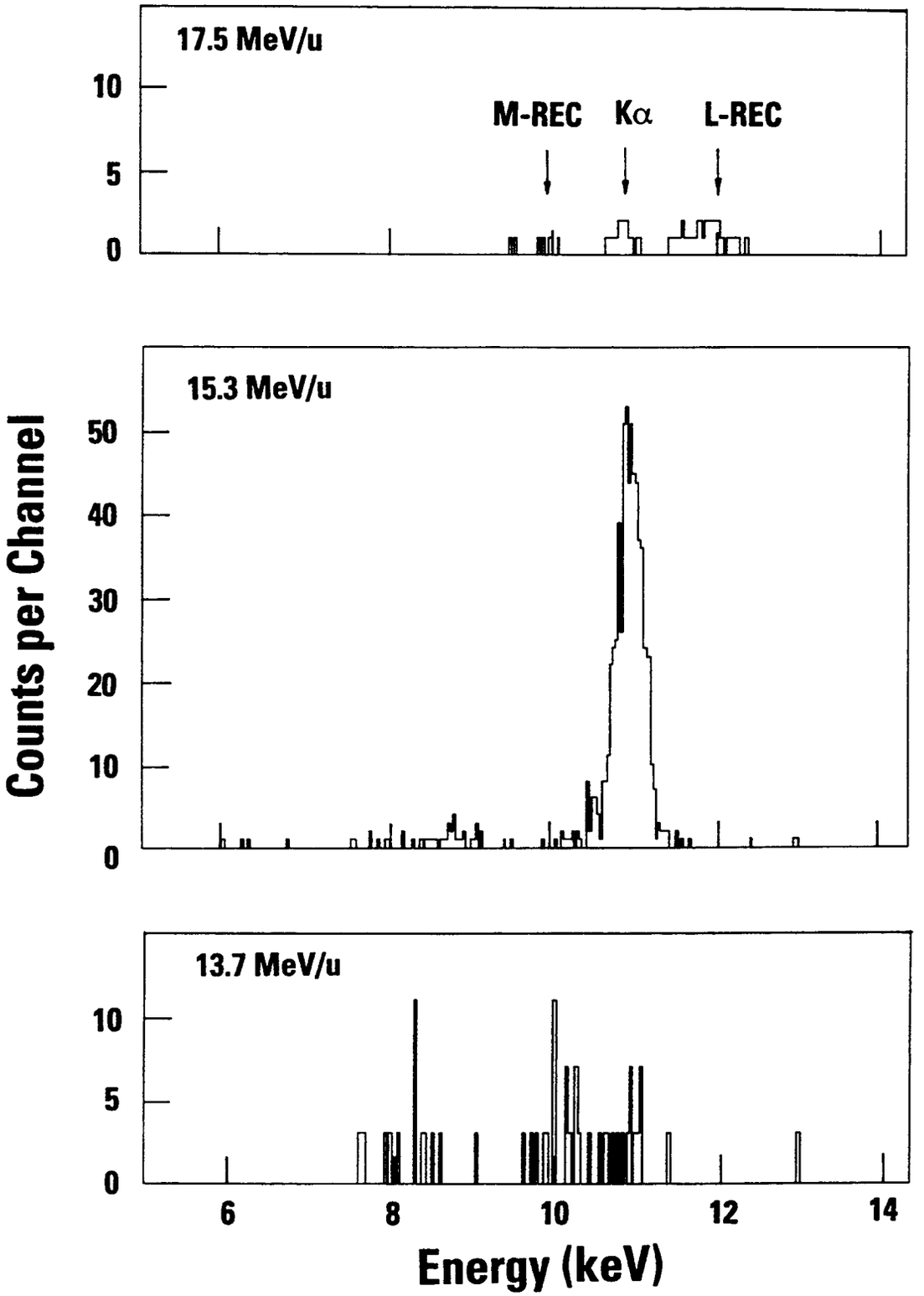
17.5 MeV/u
M-REC
Kα
L-REC
15.3 MeV/u
13.7 MeV/u
Counts per Channel
Energy (keV)
0
5
10
20
30
40
50
6
8
10
12
14

Fig. 9

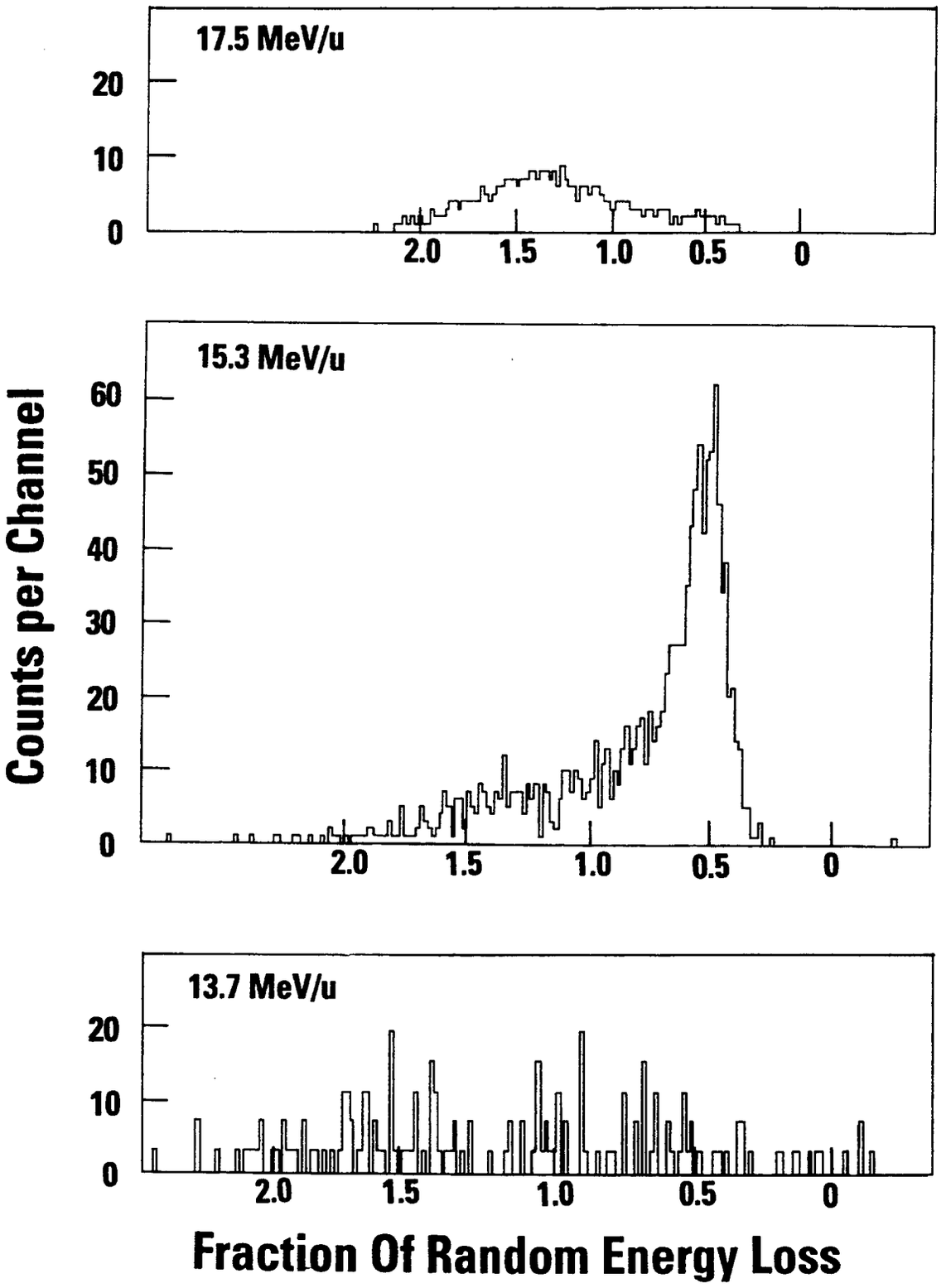
17.5 MeV/u
20
10
0
2.0
1.5
1.0
0.5
0
15.3 MeV/u
60
50
40
30
20
10
0
2.0
1.5
1.0
0.5
0
13.7 MeV/u
20
10
0
2.0
1.5
1.0
0.5
0
Counts per Channel
Fraction Of Random Energy Loss

Fig. 10